Molecular Recognition between a New Pentacyclic Acridinium Salt and DNA Sequences Investigated by Optical Spectroscopic Techniques, Proton Nuclear Magnetic Resonance Spectroscopy, and Molecular Modeling†

Clare E. Bostock-Smith,‡ Elena Giménez-Arnau,§,|| Sotiris Missailidis,§ Charles A. Laughton,§ Malcolm F. G. Stevens,*,§ and Mark S. Searle*,‡

Department of Chemistry and Cancer Research Laboratories, School of Pharmaceutical Sciences, University of Nottingham, Nottingham NG7 2RD, United Kingdom

Received October 29, 1998; Revised Manuscript Received January 28, 1999

ABSTRACT: A pentacyclic acridine, 1*H*-2,3-dihydroindolizino[7,6,5-*kl*]acridinium chloride (**1**), related in structure to tetra- and pentacyclic marine natural products, has previously been shown to induce apoptosis in breast and non-small-cell lung tumor cell lines and shows significant differences in biological potency and antitumor profile from other intercalating agents based on the acridine framework. We report on the molecular recognition of the acridinium salt with DNA, quantified by optical spectroscopic methods, and have compared these results with the clinical agent amsacrine (*m*-AMSA). The results point to an intercalative association between **1** and G−C-rich sequences of DNA. We have synthesized a hexamer duplex d(ACGCGT)$_2$, presenting two potential 5′-CpG recipient sites, and have investigated in detail by NMR and molecular modeling methods the orientational preferences of **1**, particularly with regard to the pyrrolidine ring system. On the basis of the intermolecular nuclear Overhauser effect (NOE) data, four possible intercalation models were considered; no single model produced a significantly better fit than any of the others. The best fit to the experimental data was obtained by considering a dynamic equilibrium between the different intercalated orientations with the drug maximizing π-overlap with the G−C base pairs at the intercalation site. We found little evidence for any degree of groove specificity imparted by the pyrrolidine ring. If these simulations have biological relevance they suggest that, at most, the agent induces only a transitory hot spot in the DNA which, evidently, is sufficient to be sensed by damage-recognition mechanisms of the cell.

The acridine ring system is one of the medicinal chemist's favorite molecular templates that can be decorated with a range of simple or extravagant substituents (*1*). In addition to their synthetic accessibility, derivatives of acridine are colored, stable, usually fluorescent, and exhibit a broad range of chemotherapeutic properties against procaryotic and eucaryotic cells because of the facility with which they interact with DNA targets (*2*). Notably, DNA-binding antitumor acridines disorganize topoisomerase II (*3*, *4*), a protein overexpressed in many human tumor types, such as breast cancer (*5*): however, differential selectivity toward topoisomerase α- or β-isoforms, or inhibition of other DNA-processing enzymes such as polymerases and telomerase, might contribute to their overall biological properties.

Antitumor acridines and other topoisomerase II inhibitors are also known to induce apoptotic cell death in susceptible cell lines (*6*). Starting from the point of drug administration, we are endeavoring to track how the physicochemical perturbation of DNA is recognized as damage and subsequently engages the p53-mediated induction of cell cycle arrest and/or programmed cell death (*7*). While it is easy to understand how *covalent* modification of DNA through the drug-induced formation of DNA strand breaks, DNA−DNA cross-links, or DNA−protein cross-links can be recognized by the cellular DNA damage-surveillance systems, for example by the DNA-dependent protein kinase (DNA-PK) acting upstream of p53 (*8*), it is more challenging to conceive how *noncovalent* interactions, such as intercalation or groove binding, might be so recognized, particularly when the interaction is no more than a brief encounter.

To further progress these studies we have synthesized a series of tetra- and pentacyclic acridines related in structure to marine natural products (*9*−*11*) and evaluated their interactions with DNA by physicochemical methods (*12*, *13*). One such compound, 1*H*-2,3-dihydroindolizino[7,6,5-*kl*]-acridinium chloride (**1**) (Figure 1), has desirable pharmaceutical properties in terms of stability and solubility in water (*10*). We have reported our preliminary observations that this salt potently induces apoptosis in breast and non-small-cell

† We thank the following for financial support: EPSRC (to C.E.B.-S.); a Human Capital and Mobility grant from the European Commission (to E.G.-A.); the Cancer Research Campaign, U.K. (to S.M. and M.F.G.S.); the Department of Chemistry (to M.S.S.), and the University of Nottingham for New Lecturers Awards to M.S.S. and C.A.L.

* Corresponding authors: email mark.searle@nottingham.ac.uk and malcolm.stevens@nottingham.ac.uk.

‡ Department of Chemistry.

§ Cancer Research Laboratories, School of Pharmaceutical Sciences.

|| Present address: Chargé de Recherche au CNRS, Laboratoire de Dermatochimie (CNRS, UMR 7509), Clinique Dermatologique, CHU, F-67091 Strasbourg Cedex, France.

10.1021/bi9825807 CCC: $18.00
Published on Web 05/07/1999

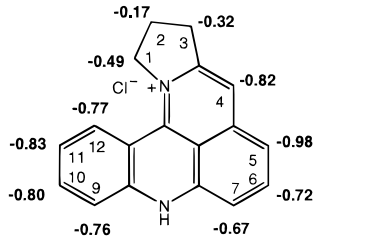

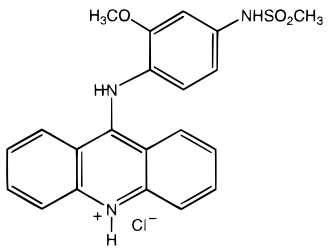

FIGURE 1: Structures of **1**, 1*H*-2,3-Dihydroindolizino[7,6,5-*kl*]-acridine chloride, and **2**, amsacrine (*m*-AMSA). Proton chemical shift differences between free and bound forms of **1** are shown in boldface type.

lung tumor cell lines irrespective of the p53 status of the lines and that there are significant differences between the biological potency and antitumor profile of the new agent and other intercalating agents (*14*) based on the acridine framework.

We report on the molecular recognition of the acridinium salt with DNA quantified by optical spectroscopic methods: in a number of cases we have compared these interactions with those of the clinically used agent amsacrine (*m*-AMSA; **2**). This work points clearly to an intercalative association between **1** and G−C rich sequences of DNA. To probe this interaction in detail we have synthesized a hexamer duplex $d(ACGCGT)_2$, presenting two potential 5′CpG recipient sites, and have studied the binding of **1** by high-field NMR and molecular modeling methods.

MATERIALS AND METHODS

Materials. The synthesis of 1*H*-2,3-dihydroindolizino-[7,6,5-*kl*]acridinium chloride (**1**) has been described earlier (*10*). Amsacrine (**2**) (*m*-AMSA; hydrochloride salt) and ethidium bromide were purchased from Sigma Chemical Co. Ltd. (Dorset, England). The DNA from salmon testes (ST-DNA; highly polymerized sodium salt, 58.8% A−T and 41.2% G−C) together with the double stranded alternating $poly(dAT)_2$, $poly(dGC)_2$, and nonalternating poly(dA)·poly-(dT) and poly(dG)·poly(dC) polymers (Sigma) were used as received. Their concentrations were determined by applying molar extinction coefficients of 6600, 6600, 8400, 6000, and 7400 M^{-1} cm^{-1} at 260 nm, respectively, and expressed in base pairs (*15*).

Optical spectroscopic experiments were conducted at pH 7.0, at which compound **1** is fully protonated ($pK_a = 9.77$) (*16*). Buffered aqueous stock solutions of the DNA samples (5 mM) were prepared in 0.2 mM filtered double-distilled water containing 10 mM sodium phosphate and 1 mM ethylenediaminetetraacetic acid (EDTA) (pH 7.0). Stock solutions of **1** (5 mM) were prepared in the same buffer at pH 7.0. Stock solutions of *m*-AMSA (5 mM) were prepared in dimethyl sulfoxide (DMSO). Drug and DNA working solutions were prepared by dilution of the stock solutions and buffered at pH 7.0 with the buffer solution described above. In the case of *m*-AMSA, the volume of DMSO in the final drug solution never exceeded 1%.

The hexamer duplex $d(ACGCGT)_2$ was synthesized on a 10 μM scale by standard solid-phase phosphoramidite chemistry and purified as previously described (*17*). The hexamer (4.3 mg) was dissolved in 550 μL of D_2O to give a 2.1 mM duplex solution. The sodium salt of trimethylsilyl propionate was added as an internal reference compound, 0.1% sodium azide as an antibacterial agent, and 0.1% EDTA to complex heavy metal ions. The hexamer was shown to be >95% pure by ^1H NMR spectroscopy.

Instrumentation. UV spectra were recorded on a Pharmacia Biotech Ultrospec 2000 UV/visible spectrophotometer. Fluorescence emission spectra were measured on a Perkin-Elmer LS-5B luminescence spectrophotometer. NMR data were collected at 500 MHz on a Bruker DRX500 spectrometer and processed on an R4600PC Silicon Graphics Indy workstation running XWINNMR software. Calculations were performed on an R10000 Silicon Graphics Indigo II workstation running AMBER 4.1 software (*18*).

Absorption Spectroscopy. To study the changes in the UV−visible absorption spectrum of compound **1** on its interaction with DNA, the following general method was used. To a fixed volume (1 mL) of an aqueous drug solution (3×10^{-5} M, pH 7.0), contained in a 10 mm path length quartz cell were added different microvolumes of a DNA solution containing the same amount of the drug, up to a sufficiently high DNA:drug ratio to ensure that the drug was fully bound. An equal concentration of DNA was added to the reference cell. Aqueous solutions of **1** obeyed the Beer−Lambert law in the relevant concentration region.

Fluorescence Emission Spectroscopy. Emission spectra were obtained by titrating an aqueous buffered (pH 7.0) drug solution (2 mL, 3×10^{-5} M) with microvolumes of a DNA solution at the same concentrations of drug and buffer. Spectra were obtained with an excitation wavelength of 475 nm. Fluorescence intensity values were monitored at the emission maximum of 540 nm. Excitation and emission slit widths were 5 and 10 nm, respectively. Fluorescence intensity values were recorded every 2 nm, spectra being monitored initially with drug alone and then after each addition of DNA.

Quenching of Ethidium−DNA Fluorescence. The *Q* values for quenching (drug concentration that reduces the fluorescence of initially DNA-bound ethidium by 50%) were determined for each DNA (20 mM) in the buffer solution at pH 7.0 containing 2 mM ethidium bromide, as previously described (*19*). These concentrations were selected to effect minimal ethidium displacement and maximum drug-induced quenching of fluorescence (*20*). All measurements were made at room temperature in 10 mm path length quartz cuvettes following serial addition of aliquots of a stock drug solution (1 mM). The DNA−ethidium complex was excited at 546 nm and the fluorescence was measured at 595 nm. The compounds and their DNA-bound complexes showed neither optical absorption nor fluorescence at 595 nm and did not interfere with the fluorescence of unbound ethidium.

NMR Spectral Studies. Compound **1** was dissolved in D_2O to give solutions of concentration 0.024, 0.12, 0.6, 3, 6, and

15 mM, and 1D proton spectra were acquired at 298 K. To form the complex of compound **1** with d(ACGCGT)$_2$, 5 μL aliquots of a 60 mM solution of compound **1** were added successively to the 550 μL (1.6 mM) DNA sample until a 2:1 drug:duplex ratio was reached. The ratio was monitored by 1D proton NMR, by integration of the thymine methyl and drug methylene protons (H2a/b) and adenine H8 and drug H10 resonances.

Spectra of the free DNA and the drug−DNA complex were acquired by use of standard phase-sensitive 2D NMR pulse sequences. Nuclear Overhauser effect (NOESY) spectra of the uncomplexed DNA were acquired at mixing times of 60, 120, and 250 ms. One-dimensional (1D) proton spectra of the free DNA and the drug−DNA complex were acquired at temperatures of 283−308 K, with 5 K increments. Total correlation (TOCSY) spectra, and NOESY spectra with mixing times of 100 and 300 ms, were acquired at 298 and 308 K. For all 2D spectra, 1024 complex data points were collected for each of 400 or 512 t_1 increments with 16−32 transients for each. Spectra were zero-filled to 2K × 1K prior to Fourier transformation. A jump-and-return NOESY sequence was employed for solvent suppression in 90% H_2O solutions and spectra were acquired at 298 and 308 K with mixing times of 300 ms.

Molecular Modeling. The starting (canonical B-form) structure of the hexamer duplex was generated by the NUCGEN module of AMBER 4.1 (*18*). Hydrogens were added with the PROTONATE module. By use of the EDIT module, explicit net-neutralizing sodium counterions were placed at the phosphates and the structure was then surrounded by a periodic box of TIP3P water molecules such that no solute atom was less than 5 Å from any box face. This led to a periodic box of size approximately 40 × 40 × 40 Å, containing 3570 water molecules. All simulations were run with the SANDER module of AMBER 4.1 and the AMBER 95 force field. SHAKE (*21*) (tolerance 0.0005 Å) was applied to all bonds, a 2 fs time step was used, and a temperature of 300 K was maintained through Berendsen temperature coupling (*22*). An 8 Å cutoff was applied to the Lennard-Jones interactions and the nonbonded list was updated every 25 steps. Molecular dynamics simulations were performed at constant pressure with isotropic position scaling and a time constant of 0.2 ps. Structure **1** was built with INSIGHT II (Biosym/MSI, San Diego, CA), and ESP-derived atomic partial charges were determined by a semiempirical approach within MOPAC (*23*) by the AM1 method. Atom types were assigned according to the AMBER 95 force field guidelines. The DNA intercalation sites were created by applying distance restraints between selected atom pairs in the flanking base pairs to give an inter-base-pair distance of 7.0−7.4 Å. The restraints were introduced over the first 5 ps of a 30 ps run at 300 K, which was cooled to 1 K over the final 5 ps. Before the drug was docked, the water and counterions were removed from the DNA. The drug was docked by use of the LEaP module of AMBER 4.1. Counterions were added to neutralize the system (8 Na^+) and the system was solvated and equilibrated. Equilibration was performed by first holding the positions of the DNA, drug molecules, and counterions fixed and running 5000 steps of minimization on the water alone followed by 5000 steps of minimization on the whole system. This was followed by 10 ps of dynamics on the water alone performed at 100 K, with the DNA and drug molecules restrained to their initial coordinates with a force constant of 100 kcal mol^{-1} Å^{-2}. After this initial equilibration, all subsequent simulations were run using the particle mesh Ewald (PME) method within AMBER 4.1. Dynamics (10 ps) was run on the water and counterions at 100 K before the system was heated to 300 K over 10 ps; equilibration was then continued as the restraints placed on the DNA were reduced to 50, 25, 12.5, 5, and finally 2.5 kcal mol^{-1} Å^{-2} in successive 10 ps runs. Each complex was subjected to 50 ps of unrestrained dynamics, first with the DNA coordinates frozen, and second allowing all molecules to move freely. Snapshots were collected at 0.5 ps intervals and average structures were calculated over the final 20 ps of the run. The complexes were judged by RMSD from starting structure to be equilibrated after 25 ps. Distances between drug and DNA protons were calculated and averaged over the final 25 ps of the trajectory.

RESULTS

UV Spectral Changes Induced by Nucleic Acids. Addition of natural ST-DNA to a solution of compound **1** induced significant changes in its absorption spectrum that were characterized by hypochromicity and accompanied by bathochromic shifts. Upon addition of ST-DNA, 68% hypochromism at all wavelengths was observed. The absorption peaks of the free ligand remained unshifted up to a 1:1 DNA:drug ratio, whereas the 475 nm absorption peak was red-shifted to 488 nm at higher DNA:drug ratios. The observation of several isosbestic points (data not shown) indicated the presence of either a single spectroscopically detectable bound species or several bound species with very similar spectroscopic features (see below). The binding of **1** to other polynucleotides, poly(dAT)$_2$, poly(dGC)$_2$, poly(dA)·poly(dT), and poly(dG)·poly(dC), presented features similar to those described above. The DNA-induced hypochromicities were roughly comparable (30−44%) and an isosbestic point at 518 nm was found in all cases.

Binding affinities of the compound **1**−DNA complexes were assessed by absorbance titrations. The spectrophotometric data allowed the values of r (molecules of ligand bound per nucleotide) and c (ligand free in the system) to be calculated (*24*). Scatchard analysis of the data gave binding isotherms (Figure 2) that were fitted to the McGhee and von Hippel neighbor-excluded site model (*25*), generalized to include more than one binding species and/or drug interaction:

$$\frac{r}{c} = K(1 - nr)\left[\frac{(2\omega - 1)(1 - nr) + r - R}{2(\omega - 1)(1 - nr)}\right]^{n-1}\left[\frac{1 - (n + 1)r + R}{2(1 - nr)}\right]^{2}$$

$$R = [[1 - (n + 1)r]^2 + 4\omega r(1 - nr)]^{1/2}$$

where r is the binding ratio, c is the concentration of unbound drug, K is the equilibrium binding constant, n is the number of base pairs occluded per bound drug molecule and ω is the cooperativity between drug binding sites. Values of $\omega > 1$ correspond to cooperative interactions, while values of $\omega < 1$ indicate anticooperativity.

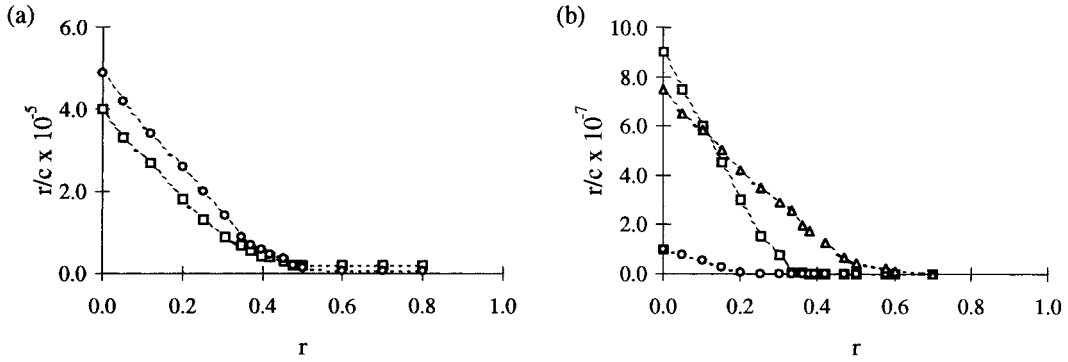

FIGURE 2: Binding isotherms for compound **1** with various DNA polymers showing plots of *r*/*c* versus *r*, where *r* is the number of molecules of drug bound per nucleotide and *c* is the concentration of free ligand. Panel a: (□) ST-DNA, (○) poly(dAT)$_2$. Panel b: (□) poly(dGC)$_2$, (○) poly(dA)·poly(dT), (△) poly(dG)·poly(dC).

Table 1: Binding Parameters of Compound **1** Complexed with ST-DNA and a Variety of Synthetic DNA Polymers

	K^a (M^{-1})	n (bp)^b	ω
ST-DNA	4.0×10^5	1.57	0.51
poly(dAT)$_2$	4.9×10^5	1.26	0.18
poly(dGC)$_2$	9.0×10^7	2.30	0.35
poly(dA)·poly(dT)	1.0×10^7	3.00	0.35
poly(dG)·poly(dC)	7.5×10^7	1.55	0.23

[a] The estimated error in the association constants is ± 10%. [b] bp = base pairs.

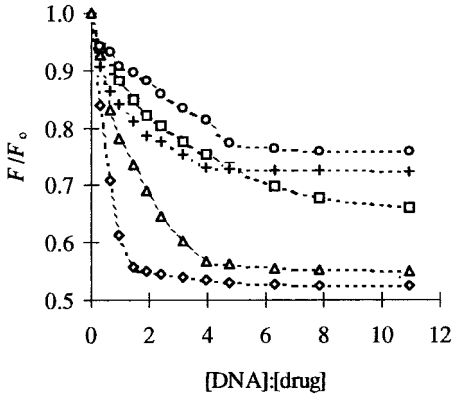

FIGURE 3: Fluorometric titration data for **1** with various polynucleotides: (□) ST-DNA, (○) poly(dAT)$_2$, (◇) poly(dGC)$_2$, (+) poly(dA)·poly(dT), and (△) poly(dG)·poly(dC). F/F_0 is plotted against the DNA:drug ratio, where F is the fluorescence of drug quenched with DNA and F_0 is the fluorescence of free drug.

The binding constants for **1** with different DNA polymers have been determined from these analyses (Table 1). The data indicated that compound **1** is a relatively strong DNA binding ligand with a DNA affinity similar to that of *m*-AMSA to ST-DNA ($K = 5.5 \times 10^5$ M^{-1}) (*26*) but lower than that of proflavine [$K = (3.0 \pm 0.5) \times 10^6$ M^{-1}] (*27*) at physiological pH. The smaller binding constants for the complexes of compound **1** with poly(dAT)$_2$ and poly(dA)·poly(dT) compared with poly(dGC)$_2$ and poly(dG)·poly(dC), respectively, indicated a G−C base-pair binding preference.

Fluorescence Emission Spectroscopy. The quenching of the fluorescence of the acridinium salt **1** at constant concentration with increasing concentrations of DNA has been studied. A plot of F/F_0, where F is the fluorescence of drug quenched with DNA and F_0 is the fluorescence of the free drug, versus DNA:drug ratio is shown in Figure 3. The data indicate that the fluorescence of **1** is differently quenched by the various polynucleotides tested. Compound **1** showed a 34% decrease in fluorescence when bound to ST-DNA. The quenching of the fluorescence was more significant upon interaction with an oligonucleotide bearing a G−C sequence [45% for poly(dGC)$_2$ and 44% for poly(dG)·poly(dC)], whereas it was less significant with A−T oligonucleotides [23% for poly(dAT)$_2$ and 27% for poly(dA)·poly(dT)]. Therefore, the fluorescence data support the spectrophotometric data in that binding of **1** to DNA shows a marked selectivity for G−C sites.

Table 2: Binding Data for **1** Determined by Ethidium−DNA Fluorescence Quenching Studies, Compared to the Reference Compound *m*-AMSA

	Q^a (μM)	
	compound **1**	*m*-AMSA[b]
ST-DNA	5.0	17.6
poly(dAT)$_2$	3.3	21.6
poly(dGC)$_2$	2.1	8.8
poly(dA)·poly(dT)	2.7	28.4
poly(dG)·poly(dC)	7.9	27.6

[a] Drug concentration to give 50% quenching of fluorescence of bound ethidium at an added ethidium:DNA molar ratio of 0.1:1 (see text); mean value from three determinations. [b] The Q value for *m*-AMSA was determined at pH 5.0 in a 10 mM sodium acetate buffer solution (1 mM EDTA).

Quenching of Ethidium−DNA Fluorescence. The fluorescence of the dye ethidium bromide is increased around 50-fold when it intercalates within DNA (*19*). Addition of a DNA binding agent induces a progressive decrease in the fluorescence of the ethidium−DNA complex. The effects of **1** on the fluorescence of the ethidium−DNA complex have been studied and compared to those of the reference compound, *m*-AMSA (**2**), at pH values where both species are in the cationic acridinium state; pH 7.0 for compound **1** ($pK_a = 9.77$) and at pH 5.0 for *m*-AMSA ($pK_a = 7.19$) (*26*). The quenching (Q) values were determined with ST-DNA or synthetic oligonucleotides to obtain further information relating to the base or sequence preference of the binding. Data are shown in Table 2. In the case of compound **1** smaller drug concentrations were necessary to reduce by 50% the fluorescence of the ethidium−DNA complex compared to *m*-AMSA, suggesting that **1** is a more effective DNA binder than *m*-AMSA itself. The data also reveal that **1** shows only slightly greater preference for poly(dGC)$_2$ over poly(dAT)$_2$ than ethidium, reflected in the small difference in Q values for binding to the two polymers (2.1 and 3.3 μM, respectively). In contrast, the Q values for binding *m*-AMSA

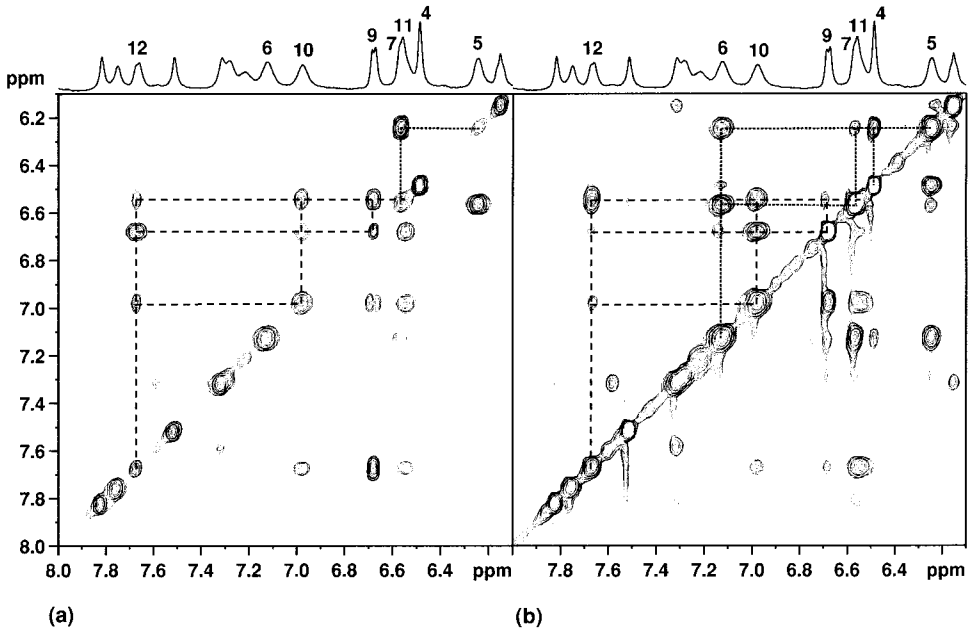

FIGURE 4: Assignment of drug resonances in the 2:1 complex of **1** with $d(ACGCGT)_2$; 1D ^1H NMR spectra are shown along the top of each 2D plot with drug resonances labeled. Connectivities within the two distinct drug spin systems, involving protons 4−7 and 9−12, are illustrated in (a) TOCSY and (b) 300 ms NOESY recorded at 308 K.

to the same polymers show a greater difference (8.8 versus 21.6 μM, respectively), indicating a significantly higher G−C selectivity than for ethidium or compound **1**.

NMR Studies. A complete assignment of free DNA ^1H resonances of the duplex $d(ACGCGT)_2$ was obtained via TOCSY and NOESY spectra. Unbound drug resonances, which had been previously assigned by 2D NOESY and 1D NOE difference spectra and coupling constants (*10*), proved to be highly concentration-dependent, indicating a degree of self-association of the pyridoacridinium salt in aqueous solution. Studies of the concentration dependence of chemical shift, and subsequent extrapolation to high dilution, provided the necessary reference state for determining shift changes upon DNA binding.

Compound **1** was titrated with $d(ACGCGT)_2$ at 298 K to a ratio of 2:1 drug:duplex. Only one set of resonances for one strand of DNA was observable at all stages of the titration at this temperature. For a symmetrical 2:1 complex, one set of DNA resonances is expected as the dyad symmetry is preserved. However, at lower ratios two or more sets of resonances are expected for a ligand in slow exchange, either representing a mixture of 2:1 and 0:1 or the asymmetric 1:1 complex or a mixture of all three, depending on the degree of binding cooperativity. The single set of resonances, which exhibit line broadening, indicates that the drug is in fast exchange between different binding sites. Variable temperature studies on the 2:1 complex showed further line broadening at temperatures below 298 K that were considerably greater than seen in studies on the duplex alone, suggesting intermediate exchange broadening at these temperatures. Moreover, at low temperature many resonances were observed to split into multiple components that were not compatible with a single symmetrical 2:1 complex in solution but multiple conformational states, suggesting the possibility of different intercalated orientations in intermediate or slow exchange. Above 298 K the lines become progressively narrower and many resonances coalesce, indicating rapid exchange between different bound states. In H_2O a large number of broadened imino proton resonances (11−14 ppm) were similarly observed at low temperature (288 K) that could not be accounted for by a simple symmetrical 2:1 binding model.

At 308 K one averaged set of bound drug signals can be identified by double quantum filtered correlation spectroscopy (DQF-COSY) and TOCSY experiments. The sharper resonances permit a full assignment of nonexchangeable signals for both the bound drug and the hexamer duplex via NOESY and TOCSY spectra (Figure 4). Line broadening was particularly evident for the G and C resonances, indicating that all four of these are involved in drug binding, consistent with the drug preferentially occupying the two CpG intercalation sites as predicted, and in agreement with the GC specificity determined by optical spectrophotometric and fluorescence quenching experiments.

Changes in chemical shifts of drug and DNA were monitored during the titration. While there was an initial large change in drug and, to a lesser extent, DNA resonances on addition of a small amount of drug, the shifts did not change further as more drug was added (with the exception of the adenine H2). The differences in chemical shifts of compound **1** between complexed (2:1 drug:duplex) and uncomplexed forms (high dilution) are significant (Figure 1). Large upfield shifts in the range −0.67 to −0.98 ppm for the protons of the aromatic pyridoacridine ring system of **1** are indicative of intercalation, with the smaller shift changes of the puckered pyrrolidinium ring implying that this is protruding into the major or the minor groove. Change in chemical shift with temperature was monitored for a number of resonances and the melting temperature of the complex was determined to be greater than 318 K.

A large number of NOEs (see Table 3) have been identified between the bound ligand and DNA protons, largely with the base and sugar protons of G3 and G5. Fewer NOEs were observed to C2 and C4 due to extensive line

Table 3: Correlation of Observed Drug−DNA NOEs with Measured Distances in Molecular Dynamics Simulations of 2:1 Complexes of **1** with d(ACGCGT)$_2$[a]

A|B / C|D	H3A H3B	H4	H5	H6	H7	H9	H10	H11	H12
C2 H1'						●			
G3 H1'		●	●			●		●	
G5 H1'		●	●			●	●	●	
G3/G5 H2' C2/C4 H2"		●	●	●	●	●	●	●	
G3 H2"		●						●	
G5 H2"							●		
G3 H4'		●		●			●	●	
G5 H4'		●			●	●	●	●	
G3/G5 H5'	●	●	●	●	●	●	●	●	●
G3/G5 H5"	●	●	●	●	●	●	●	●	●
G3 H8								●	
G5 H8								●	
C2 H5					●				
C2 H6			●		●			●	

[a] Each cross represents an observed NOE between drug and DNA protons. A black dot in any one quadrant indicates that the observed NOE is consistent with a particular binding mode (A, B, C, or D) as indicated in the key in the top left-hand corner. Average distances in each of the four possible complexes were calculated over the final 20 ps of each simulation and distances < 5 Å (within 1 standard deviation) were considered consistent with an observed NOE.

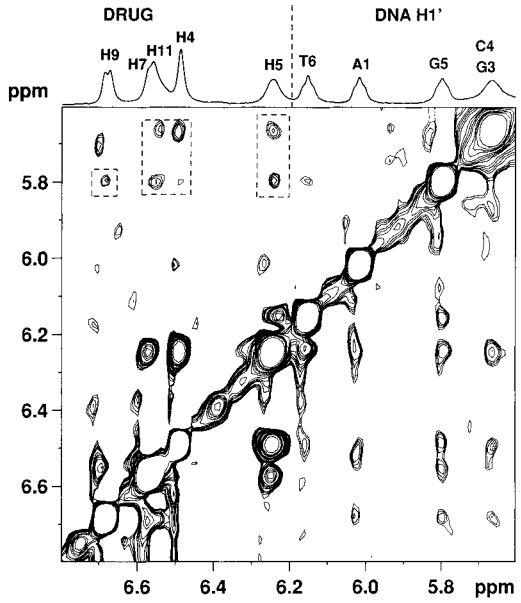

FIGURE 5: Portion of the 300 ms NOESY spectrum of the 2:1 complex of **1** with d(ACGCGT)$_2$ at 308 K showing NOEs (boxed) from drug H4, H5, H7, H9, and H11 to deoxyribose H1′ resonances. The corresponding 1D spectrum is shown along the top of the plot with assignments indicated.

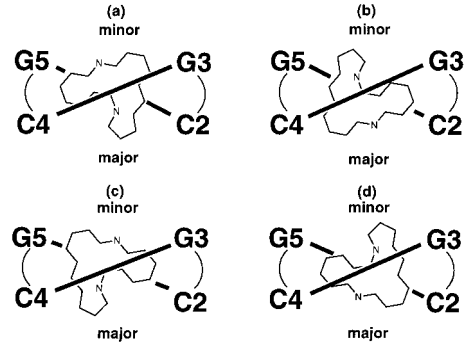

FIGURE 6: Schematic representation of four different binding modes (a−d) of **1** intercalated at the 5′ CpG steps of d(ACGCGT)$_2$. Only the outline of the pentacyclic acridine ring system is illustrated for clarity.

broadening, again consistent with exchange between different bound environments involving predominantly the CpG steps. The observation of NOEs to G5 as well as to G3 suggests a CpG rather than a GpC binding site, consistent with the evidence from differential line broadening of C2 and C4. A number of NOE cross-peaks between ligand aromatic protons and deoxyribose H1′ protons are shown (Figure 5). We cannot exclude the possibility of there being a minor population of drug molecules intercalated at the central GpC site giving rise to a subset of NOEs; however, intercalation at this site would exclude the possibility of a second bound drug on the basis of the neighboring site exclusion principle. The data are, however, consistent with predominantly CpG site intercalation. On this basis, four possible intercalative binding modes exist for each drug and are shown schematically in Figure 6. Two have the pyrrolidine ring lying in the major groove and two in the minor, each pair having a C2 rotation about the short axis of the drug. Thus, NOE cross-peak intensities represent a population-weighted average over each of these bound states.

Molecular Modeling. Preliminary modeling studies suggested that the NOE data were consistent, in part, with all four different intercalation modes at the CpG sites (Figure 6). Dynamics simulations on symmetrical models of all four binding modes resulted in four structures, each being a time-average over the final 25 ps of the simulations when the trajectories were stable. Between them they were able to account for 92% of the NOEs observed (specifically, 92% of the NOEs corresponded to a distance in one or more structures of less than 5 Å, within 1 standard deviation, once those that could be accounted for by spin diffusion or resonance overlap had been discarded). No single structure was able to account for the full 92%, while no structure could be discarded without reducing the number of NOEs accounted for. Each binding mode has its own distinguishing NOE connectivities. For example, G5 H4′ gives NOEs to acridine H7, H9, H10, and H11. Those to H9 and H10 correlate with mode A, to H7 with mode C, and to H11 with mode D. An NOE is also observed from G5 H4′ to H4 but this is not unique to a single structure (Table 3). In total, mode B only has one distinguishing NOE (G3 H2″ to H11), while modes A, C, and D have six, five, and five distinguishing NOEs, respectively. Correlation of NOEs with short distances for each binding mode is given in Table 3, showing

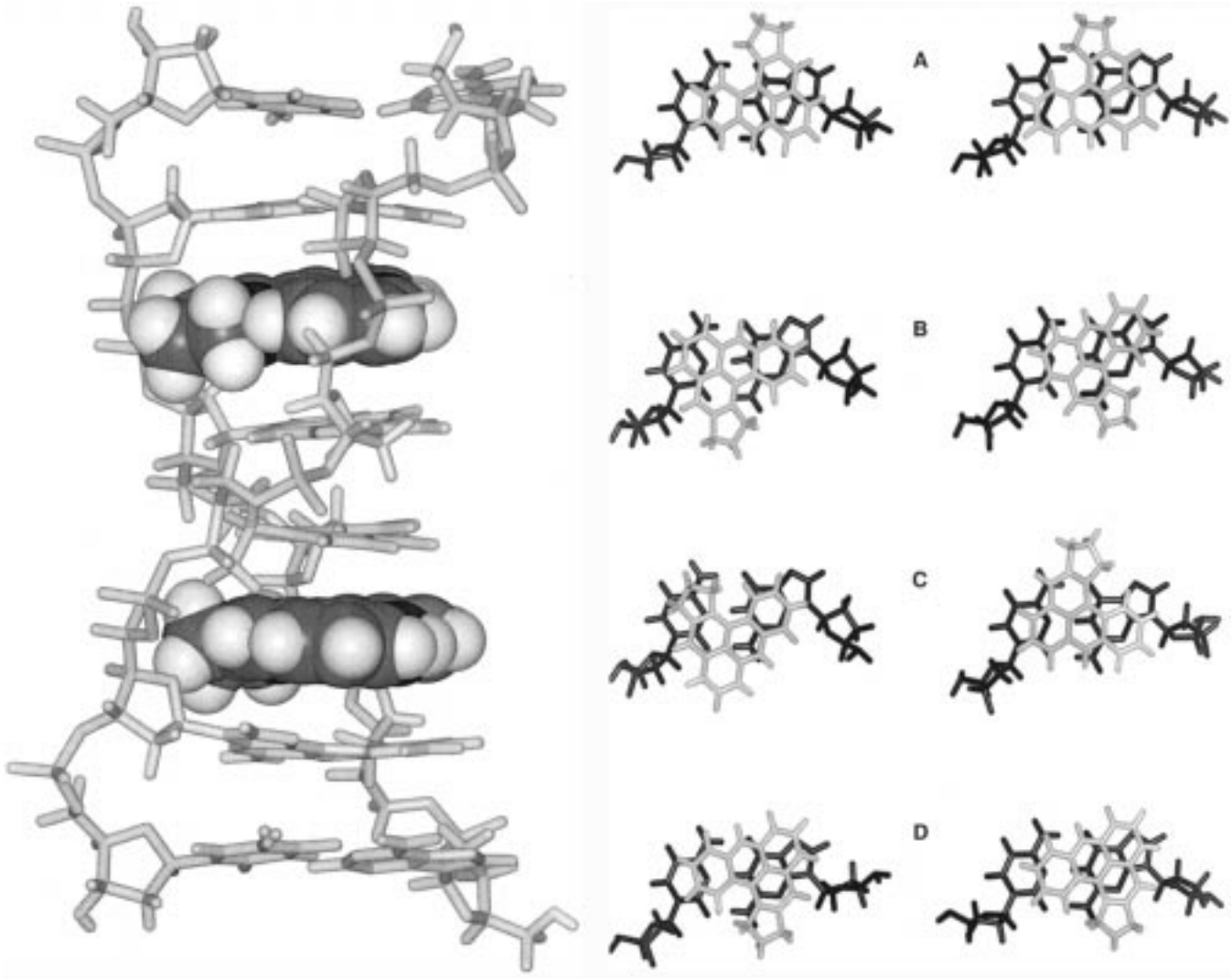

FIGURE 7: (Left panel) Binding mode A of the 2:1 complex of **1** with d(ACGCGT)$_2$; mean structure from the final 25 ps of molecular dynamics simulations of the complex. (Right panel) Binding modes A−D, illustrating stacking interactions between the drug and the 5′−G-C base pairs at each of the two intercalation sites per complex.

the even spread of NOE correlations across the four binding modes. Structures were also examined for short distances for which an NOE might have been predicted. A number of these were apparent in the four modeled complexes but could be accounted for by factors such as line broadening and signal overlap, which made assignment ambiguous.

In three of the four simulations the drug is seen to converge to the same orientation at both binding sites. These orientations can be seen to maximize overlap between the π systems of the drug and the flanking base pairs (Figure 7). This also serves to place the pyrrolidine ring in the center of the groove in which it is located, with minimal overlap with aromatic ring systems, consistent with the small chemical shift change seen on binding. In one binding mode (Figure 7, mode C), two different orientations are seen, fitting with slightly different but similar numbers of NOEs.

DISCUSSION

Physicochemical Studies of the Drug−DNA Interaction. The results from several different complementary techniques have provided information concerning the mechanism of binding of a new polycyclic acridinium salt **1** to DNA. The decrease in the absorbance at 475 nm (red-shifted to 488 nm) observed in the UV spectrum of **1** in the presence of ST-DNA was consistent with insertion of the molecule into the double helix by intercalation. Similar spectral features were induced by other synthetic DNAs of different base composition. Initially, the presence of several distinct isosbestic points in the absorbance titrations with ST-DNA suggested that only two distinct forms of the drug were in solution—the free form and one, or a number of similar, fully bound (intercalated) forms. However, the presence of an isosbestic point does not prove that there are only two forms of the drug present. The binding isotherms for the interaction between **1** and various DNA polymers are presented in Figure 2 in the form of Scatchard plots. The plots are hyperbolic and are comparable to the binding curves obtained for the interaction of *m*-AMSA (*28*) and proflavine (*29*) with natural DNA. For these reference compounds such a binding curve has been interpreted as showing two distinctly different binding modes: one of high affinity (type I) and one of lower affinity (type II). The type I process is strong and corresponds to the intercalation of the drug into the DNA double helix at low binding ratios. The type II process is weak and is normally attributed to external electrostatic binding at high binding ratios. Type I binding predominated for $r < 0.16$ in

the case of *m*-AMSA (*28*) and for $r < 0.2$ in the case of proflavine (*29*), whereas type II binding predominated for $r > 0.16$ and for $r > 0.2$, respectively. The effect of a tight binding site is dominant at $r < 0.4$ in the case of compound **1**, with weaker binding becoming prominent at $r > 0.4$. Since type I binding is associated with the intercalation of the acridine ring between DNA base pairs, we conclude that compound **1** is a more effective DNA intercalating agent than either *m*-AMSA or proflavine.

For ligands such as intercalating drugs, which are subject to neighboring site exclusion effects, precise binding parameters cannot be determined by traditional Scatchard plots, since the total number of binding sites is not independent of the binding ratio. We calculated the apparent binding constants (K) and the site size n for the interaction of **1** to various DNA polymers using the spectrophotometric data and the excluded-site McGhee and von Hippel model (*25*). In contrast to the Scatchard treatment, binding parameters calculated by the latter model are critically dependent upon the choice of lattice unit. For intercalating agents such as *m*-AMSA and simple aminoacridines it is reasonable to assume that the concentration of potential binding sites in the naked lattice corresponds to the concentration of inter-base-pair regions in double-stranded DNA. Consequently, we have expressed the concentration of binding sites and the binding ratios in terms of base pairs. The extended McGhee and von Hippel equation (*25*), incorporating cooperativity (see Results section), has been chosen for the analysis of the data instead of the simpler known equation: $r/c = K(1 - nr)[(1 - nr)/(1 - (n - 1)r]^{n-1}$. The introduction of a drug cooperativity factor (ω) modifies the theory to produce Scatchard plots that are concave. The new polycyclic acridine **1** can form aggregates (see NMR dilution experiments) at higher concentrations. The extended equation has the advantage that it provides information about drug aggregation (cooperative binding, $\omega > 1$) or noncooperative binding ($\omega < 1$, no aggregation/nearest neighbor exclusion). Values of $\omega < 1$ (see Table 1) were obtained in all cases, in agreement with noncooperative binding, as further suggested by CD studies (to be published separately). Binding parameters defined in Table 1 indicate that **1** binds strongly to ST-DNA ($K = 4.0 \times 10^5$ M^{-1}) and that it is more selective for G−C-rich DNA sequences. The data show that **1** has a 200-fold higher affinity for poly(dGC)$_2$ relative to poly(dAT)$_2$ with a binding constant to the former oligonucleotide of 9.0×10^7 M^{-1}, but much poorer discrimination is observed between poly(dA)·poly(dT) and poly(dG)·poly(dC). The higher affinity for poly(dGC)$_2$ suggests that G−C-rich alternating pyrimidine−purine sequences represent the preferred DNA binding site for **1** and binding parameters confirm site sizes close to two base pairs ($n \leq 2$), indicating partial or complete intercalation of the drug within the DNA double helix, as expected for the neighboring site exclusion model.

The fluorometric titrations agreed reasonably well with the spectrophotometric analysis results, confirming that **1** binds more tightly to poly(dGC)$_2$ than to poly(dAT)$_2$. The results for the complementary homopolymer pairs also indicate tighter drug binding to poly(dG)·poly(dC) than to poly(dA)·poly(dT). The amount of quenching increased with the DNA G−C content, indicating that G−C-containing sites are responsible for the greatest amount of quenching and, therefore, of binding. The same evidence of the high binding ability of **1** to G−C sequences was expected in the ethidium−DNA fluorescence quenching assays. However, the Q values revealed that binding was without marked base pair specificity compared with *m*-AMSA, the Q value for the interaction of **1** with poly(dGC)$_2$ being only 1.5 times smaller than with poly(dAT)$_2$. Direct observation of base pair preference by footprinting experiments was thwarted because compound **1** did not give a distinct footprint (data not shown).

NMR Spectroscopy. To probe in more detail the nature of the DNA recognition, a short oligonucleotide duplex d(ACGCGT)$_2$ was synthesized containing two symmetry-related high-affinity 5′-pyrimidine−purine (5′-CpG) steps for high-resolution NMR studies. These, and the subsequent molecular modeling studies, were not consistent with the drug binding in one preferred orientation but rather that all four possible intercalated orientations were required to account for the observed NOEs, with the pyrrolidine ring showing no particular preference for binding in either groove (Figure 6). The different intercalated conformations of the drug are in intermediate to fast exchange on the chemical shift time scale. Perturbations to ^{1}H chemical shifts have been widely used to provide a qualitative analysis of the mode of DNA binding of both intercalators and groove binders; alterations in base stacking that accompany intercalation produce characteristic chemical shift changes (*30*). Significant upfield shifts (negative $\Delta\delta$) are evident for the protons of the aromatic pyridoacridine ring system in the range −0.67 to −0.98 ppm (Figure 1), indicative of the importance of π-stacking interactions with the DNA base pairs in complex stabilization and in good agreement with two previous NMR studies of DNA−acridine complexes (*31*, *32*). In contrast, resonances from the pyrrolidine ring undergo more modest changes in shift, consistent with protrusion into the major or minor groove.

Studies both by NMR and by footprinting methods have shown that simple acridines tend to show no orientational specificity (*33*); however, ring substituents can alter this behavior (*34*). There has been a degree of controversy over the orientation of *m*-AMSA, with some claims for the anilino ring to lie preferentially in the minor groove and some for the major groove (*33*). Among the more highly substituted examples, acridine−triazene combilexins bind with the anilino ring and its pendant triazene moiety lying in the minor groove (*35*), while a cobalt(III)−bleomycin analogue also tethered to the 9 position lies in the major groove (*31*). More unusually, an acridine with a spermine at the 9 position is proposed to intercalate asymmetrically, stacking between just the purines of a purine−purine site with the spermine protecting the pyrimidine strand from cleavage (*34*). Further embellishment of the new acridinium salt **1** with pendant substituents capable of groove-specific interactions, or modifications to the pyrrolidine fragment, may facilitate better sequence and orientational discrimination.

The combination of spectrophotometric and NMR data allows us to draw some conclusions regarding the nature of the binding of compound **1** to DNA and how base sequence might influence this binding. Binding of **1** to DNA appears to be similar to that of other aminoacridine derivatives, in that two types of binding site (type I and type II) were observed. An intercalative process (type I) of the acridinyl moiety has been demonstrated for **1**, conferring high DNA

binding affinity. The weak binding process (type II) could be attributed to an external electrostatic attraction at high binding ratios. With regard to sequence selectivity, spectrophotometric and fluorometric analyses suggest a strong G−C base pair preference of the drug. NMR and molecular modeling studies demonstrate intercalation at CpG sites while also showing that compound **1** is in fast exchange on the NMR time scale between a number of bound conformations with no observed orientational specificity. The NMR studies in particular highlight the dynamic nature of the recognition process between **1** and DNA. If these simulations have biological relevance they suggest that, at most, the agent induces only a transitory hot spot in the DNA that, evidently, is sufficient to be sensed by damage-recognition mechanisms of the cell.

REFERENCES

1. Albert, A. (1966) *The Acridines*, 2nd ed., Edward Arnold (Publishers) Ltd., London.
2. Denny, W. A., and Baguley, B. C. (1994) in *Molecular Aspects of Anti-Cancer Drug−DNA Interaction* (Neidle, S., and Waring, M. J., Eds.) pp 270−311, Macmillan, London.
3. Baguley, B. C. (1991) *Anti-Cancer Drug Des. 6*, 1−36.
4. Kohn, K. W. (1996) *Cancer Res. 56*, 5533−5546.
5. Houlbrook, S., Addison, C. M., Davies, S. L., Carmichael, J., Stratford, I. J., Harris, A. L., and Hickson, I. D. (1995) *Br. J. Cancer 72*, 1454−1461.
6. Negri, C., Bernardi, R., Donzelli, M., and Scovassi, A. I. (1995) *Biochimie 77*, 893−899.
7. Harris, C. C. (1996) *J. Natl. Cancer Inst. 88*, 1442−1555.
8. Woo, R. A., McLure, K. G., LeesMiller, S. P., Rancourt, D. E., and Lee, P. W. K. (1998) *Nature 394*, 700−704.
9. Hagan, D. J., Giménez-Arnau, E., Schwalbe, C. H., and Stevens, M. F. G. (1997) *J. Chem. Soc., Perkin Trans. 1*, 2739−2746.
10. Hagan, D. J., Chan, D., Schwalbe, C. H., and Stevens, M. F. G. (1998) *J. Chem. Soc., Perkin Trans. 1*, 915−929.
11. Julino, M., and Stevens, M. F. G. (1998) *J. Chem. Soc, Perkin Trans. 1*, 1677−1684.
12. Giménez-Arnau, E., Missailidis, S., and Stevens, M. F. G. (1998) *Anti-Cancer Drug Des. 13*, 125−143.
13. Giménez-Arnau, E., Missailidis, S., and Stevens, M. F. G. (1998) *Anti-Cancer Drug Des. 13*, 431−451.
14. Stanslas, J., Marsh, K. L., Austin, C. A., Robins, R. A., Price, M. R., Double, J. A., and Stevens, M. F. G. (1998) *Br. J. Cancer 78*, (S1), P32.
15. Plouvier, B., Houssin, R., Helbecque, N., Colson, P., Houssier, C., Hénichart, J.-P., and Bailly, C. (1995) *Anti-Cancer Drug Des. 10*, 155−166.
16. Voet, D., and Voet, J. G. (1995) in *Biochemistry*, 2nd ed., pp 35−38, John Wiley & Sons, Inc., New York.
17. Bostock-Smith, C. E., Laughton, C. A., and Searle, M. S. (1998) *Nucleic Acids Res. 26*, 1660−1667.
18. Pearlman, D. A., Case, D. A., Caldwell, D. W., Ross, W. S., Cheatham, T. E., III, Ferguson, D. M., Siebel, G. L., Singh, C., Weiner, P. K., and Kollman, P. A. (1995) *Amber 4.1*, University of California, San Francisco, CA.
19. Bailly, C., Pommery, N., Houssin, R., and Hénichart, J.-P. (1989) *J. Pharm. Sci. 78*, 910−917.
20. Morgan, A. R., Lee, J. S., Pulleyblank, D. E., Murray, N. L., and Evans, D. H. (1979) *Nucleic Acids Res. 7*, 547−569.
21. Ryckaert, J. P., Ciccotti, G., and Berendsen, H. J. C. (1977) *J. Comput. Phys. 23*, 327−341.
22. Berendsen, H. J. C., Postma, J. P. M., van Gunsteren, W. F., DiNola, A., and Haak, J. R. (1984) *J. Comput. Phys. 81*, 3684−3690.
23. Stewart, J. P. P. Mopac 6.0 (QCPE), available from the Quantum Chemistry Program Exchange, Indiana University, Bloomington, IN.
24. Peacocke, A. R., and Skerrett, J. N. H. (1956) *Trans. Faraday Soc. 52*, 261−279.
25. McGhee, J. D., and von Hippel, P. H. (1974) *J. Mol. Biol. 86*, 469−489.
26. Denny, W. A., Atwell, G. J., and Baguley, B. C. (1983) *J. Med. Chem. 26*, 1625−1630.
27. Armstrong, R. W., Kurucsev, T., and Strauss, U. P. (1970) *J. Am. Chem. Soc. 92*, 3174−3181.
28. Gormley, P. E., Sethi, V. S., and Cysyk, R. L. (1978) *Cancer Res. 38*, 1300−1306.
29. Blake, A., and Peacocke, A. R. (1968) *Biopolymers 6*, 1125−1253.
30. Sartorius, J., and Schneider, H. J. (1997) *J. Chem. Soc., Perkin Trans. 2*, 2319−2327.
31. Tan, J. D., Farinas, E. T., David, S. S., and Mascharak, P. K. (1994) *Inorg. Chem. 33*, 4295−4305.
32. Gaugain, B., Markovits, J., Lepecq, J. B., and Roques, B. P. (1981) *Biochemistry 20*, 3035−3042.
33. Bailly, C., Denny, W. A., Mellor, L. E., Wakelin, L. P. G., and Waring, M. J. (1992) *Biochemistry 31*, 3514−3524.
34. Blagbrough, I. S., Taylor, S., Carpenter, M. L., Novoselskiy, V., Shamma, T., and Haworth, I. S. (1998) *Chem. Commun.*, 929−930.
35. McConnaughie, A. W., and Jenkins, T. C. (1995) *J. Med. Chem. 38*, 3488−3501.

BI9825807